

MOLECULAR CLUMPS DISGUIISING THEIR STAR-FORMATION EFFICIENCY PER FREE-FALL TIME: WHAT WE CAN DO NOT TO BE FOOLED

GENEVIÈVE PARMENTIER¹
Accepted to ApJ

ABSTRACT

The presence of a volume density gradient in molecular clumps allow them to raise their star formation rate compared to what they would experience were their gas uniform in density. This higher star formation rate yields in turn a higher value for the star formation efficiency per freefall time that we measure. The measured star formation efficiency per freefall time $\epsilon_{\text{ff, meas}}$ of clumps is therefore plagued by a degeneracy, as two factors contribute to it: one is the density gradient of the clump gas, the other is the intrinsic star formation efficiency per freefall time $\epsilon_{\text{ff, int}}$ with which the clump would form stars should there be no gas density gradient. This paper presents a method allowing one to recover the intrinsic efficiency of a centrally-concentrated clump. It hinges on the relation between the surface densities in stars and gas measured locally from clump center to clump edge. Knowledge of the initial density profile of the clump gas is not required. A step-by-step description of the method is provided as a tool in hand for observers. Once $\epsilon_{\text{ff, int}}$ has been estimated, it can be compared with its measured, clump-averaged, counterpart $\epsilon_{\text{ff, meas}}$ to quantify the impact that the initial gas density profile of a clump has had on its star formation history.

Subject headings: Star formation (1569); Molecular clouds (1072); Star clusters (1567)

1. INTRODUCTION

Molecular clumps whose gaseous component presents a volume density gradient experience a higher star formation rate than if their gas was of uniform density (Tan et al. 2006; Girichidis et al. 2011; Elmegreen 2011; Parmentier 2014, 2019). This property stems from the inner-regions of centrally-concentrated clumps forming stars at a pace faster than expected based on the clump mean freefall time. Their density is actually higher than the clump mean density. Parmentier (2019) introduces the notion of *magnification factor*, ζ , defined as the factor by which the density gradient of a clump inflates its star formation rate. In other words, this is the ratio between the star formation rate of a clump with a density gradient, SFR_{clump} , and the star formation rate that the same clump would present in the absence of it, SFR_{TH} ('TH' stands for the 'top-hat' profile of uniform-density gas). She shows that ζ depends on the power-law slope of the gas density profile and on the fractional extent of its central core: the steeper the slope, the smaller the radius of the central core as compared to the clump radius, the higher the magnification factor ζ .

The density gradient inside molecular clumps also impacts their star formation efficiency per freefall time as we measure it, since it depends on the clump star formation rate SFR_{clump} as (see e.g. Krumholz & Tan 2007; Evans et al. 2009; Lada, Lombardi & Alves 2010; Murray 2011; Krumholz, Dekel & McKee 2012; Vutisalchavakul, Evans & Heyer 2016; Ochsendorf et al. 2017):

$$\epsilon_{\text{ff, meas}} = \frac{SFR_{clump} \langle \tau_{\text{ff}} \rangle}{m_{\text{gas}}}. \quad (1)$$

In this equation, m_{gas} and $\langle \tau_{\text{ff}} \rangle$ are the gas mass and gas

mean free-fall time of the clump, respectively. A density gradient therefore also inflates the star formation efficiency per freefall time as compared to what would be measured for a top-hat profile. Parmentier (2019) refers to the efficiency that would be measured for a top-hat profile as the *intrinsic* star formation efficiency per free-fall time, $\epsilon_{\text{ff, int}}$, to emphasize that $\epsilon_{\text{ff, int}}$ is unaffected by the density gradient. $\epsilon_{\text{ff, int}}$ also characterizes the star formation activity of the nested shells of gas of which the clump is made, as long as these shells are thin enough to be considered of uniform density (see Equation 4 in Parmentier 2019). The measured star formation efficiency per freefall time derived from Equation 1 by observers therefore constitutes a global quantity, while its intrinsic counterpart is a local quantity. How to reveal the latter is the main objective of this paper. All these parameters are intertwined through her Equation 10, which we reproduce here for the sake of clarity:

$$\zeta = \frac{SFR_{clump}}{SFR_{TH}} = \frac{\epsilon_{\text{ff, meas}}}{\epsilon_{\text{ff, int}}}. \quad (2)$$

A crucial consequence is that even if the intrinsic star formation efficiency per freefall time $\epsilon_{\text{ff, int}}$ were universal (that is, no variations from clump center to clump edge, and no inter-clump variations), the measured star formation efficiency per freefall time $\epsilon_{\text{ff, meas}}$ would present wide fluctuations. Such fluctuations, embodied by the ζ factor, reflect the diversity in clump structures rather than variations in the physics of star formation. Observations of molecular clumps of the Galactic disk show that the logarithmic slope of their power-law density profile varies from $\simeq -1$ down to $\simeq -4$ (e.g. Müller et al. 2002; Schneider et al. 2015). The steepest density profiles (slope equal to or steeper than -3) are observed in dense pc-size regions of nearby molecular clouds (Schneider et al. 2015). For such steep density profiles, Parmentier (2019) shows that the magnification factor

¹ Astronomisches Rechen-Institut, Zentrum für Astronomie der Universität Heidelberg, Mönchhofstr. 12-14, D-69120 Heidelberg, Germany

can boast more than one order of magnitude depending on the central peakedness of the gas density profile, that is, depending on the profile slope and on the extent of the central core (see her Section 5).

Global observations of molecular clumps therefore leave us with an annoying degeneracy, for how can we disentangle in the measured star formation efficiency per freefall time $\epsilon_{\text{ff,meas}}$ the impact of the density gradient (i.e. ζ) from the contribution of the star formation process *per se* (i.e. $\epsilon_{\text{ff,int}}$)? For instance, consider a clump whose measured star formation efficiency per freefall time is $\epsilon_{\text{ff,meas}} = 0.10$. How should it be interpreted? Does it imply that any small region of the clump forms stars with an (intrinsic) star formation efficiency per freefall time of $\epsilon_{\text{ff,int}} = 0.10$? Or is this efficiency smaller (e.g. $\epsilon_{\text{ff,int}} = 0.02$), with the "missing" factor 5 being contributed by the clump density gradient?

Parmentier (2019) mapped the magnification factor ζ of model clumps as a function of time and for a range of conditions at star formation onset. These conditions are, for each model clump, its mass, radius, volume density profile, and intrinsic star formation efficiency per free-fall time. In this contribution, we consider the reversed problem: given a model clump at time t after star formation onset, how can we recover its intrinsic star formation efficiency per free-fall time? That is, the goal is now to quantify $\epsilon_{\text{ff,int}}$ in clumps with ongoing star formation, where the initial gas distribution has been altered by star formation. We will show how spatially-resolved observations can help us break the degeneracy existing between ζ and $\epsilon_{\text{ff,int}}$, with the additional advantage of using gas and star projected/surface densities, which are more easily measured than spatial/volume densities. Once estimated, $\epsilon_{\text{ff,int}}$ can be combined with the "traditional" measured star formation efficiency per freefall time to quantify the impact of the clump density gradient as $\zeta = \epsilon_{\text{ff,meas}}/\epsilon_{\text{ff,int}}$.

The outline of the paper is as follows. In Section 2, we summarize the key aspects of the model of Parmentier (2019). Section 3 shows how the measured star formation efficiency per freefall time is obtained for the model clumps. In Section 4, we explain how spatially-resolved data can help us probe $\epsilon_{\text{ff,int}}$, and we introduce our method. In Section 5, we apply it to the comprehensive grid of model clumps built by Parmentier (2019). A step-by-step description of how to implement the method is presented in Section 6. Section 7 contains a brief discussion, followed by the conclusions in Section 8.

2. MODEL-PREDICTED MAGNIFICATION FACTOR

In this section, we summarize the model implemented by Parmentier (2019, hereafter Paper I) and how it predicts the magnification factor of model clumps.

The volume density profile of a model clump is described by a decreasing power-law of logarithmic slope $-p_0$ with a central core r_c so as to avoid a density singularity at the clump center (see Equation 11 in Paper I). The clump mass m_{clump} is the mass enclosed within the radius r_{clump} . The clump density profile is also the density profile of the clump gas at star formation onset ($t = 0$). Equation 19 in Parmentier & Pfalzner (2013) allows one to obtain the corresponding gas density profile at time t after star formation onset for a given in-

trinsic star formation efficiency per free-fall time. The latter is assumed to be time-invariant and $\epsilon_{\text{ff,int}} = 0.01$ is assumed in all simulations. The star formation rate SFR_{clump} of the clump is then obtained by numerically integrating the star formation rate of nested shells of gas from clump center to clump edge, the star formation activity of all shells being characterized by the intrinsic star formation efficiency per freefall time (see Equation 4 in Paper I). The gas mass m_{gas} of the clump at any time t is similarly obtained by integrating the corresponding gas volume density profile over the clump volume. The difference between the total mass of the clump m_{clump} (equivalently the gas initial mass $m_{\text{gas}}(t = 0)$) and the gas mass at time t provides the mass in stars formed over the time-span t . The global star formation efficiency (i.e. the fraction of the initial gas mass turned into stars) follows as $SFE_{\text{gl}}(t) = m_{\text{stars}}(t)/m_{\text{clump}} = (m_{\text{clump}} - m_{\text{gas}}(t))/m_{\text{clump}}$.

It is now doable to predict the corresponding magnification factor $\zeta(t)$. The model assumes that the clump radius remains constant through the star formation process, and knowledge of the gas mass m_{gas} thus yields the mean density of the gas $\langle \rho_{\text{gas}} \rangle$ and its mean free-fall time

$$\langle \tau_{\text{ff}} \rangle = \sqrt{\frac{3\pi}{32G\langle \rho_{\text{gas}} \rangle}}. \quad (3)$$

The star formation rate that the clump *would* experience in the absence of a density gradient is then given by:

$$SFR_{TH} = \epsilon_{\text{ff,int}} \frac{m_{\text{gas}}}{\langle \tau_{\text{ff}} \rangle}. \quad (4)$$

It stems from assuming a constant gas density in Equation 4 of Paper I. The model-predicted magnification factor then follows from its definition, namely, $\zeta = SFR_{\text{clump}}/SFR_{TH}$.

Color-coded maps of the magnification factor at $t = 0$ and $t = 0.5$ Myr are presented in Figures 5, 6 and 7 in Paper I for various clump masses, radii, and initial volume density profiles of the gas. A more centrally-peaked density profile - be it through a steeper slope or a smaller central core as compared to the clump radius - yields higher star formation rates and higher magnification factors. Because star formation operates fastest in the high-density regions of the clump center, the gas density profile loses part of its central peakedness as time goes by and ζ decreases as a result. The decrease is faster for models with a higher mean volume density (hence a shorter mean freefall time) and/or with a steeper slope initially (thus a higher central density).

To derive the magnification factor of model clumps at any time t is doable because we can predict the gas density profile at that time t based on our assumptions of an initial gas density profile and intrinsic star formation efficiency per free-fall time. But what about star-forming clumps of the Galactic disk, i.e. clumps observed at time $t > 0$ after star formation onset? Neither their intrinsic star formation efficiency per free-fall time, nor the initial spatial distribution of their gas is known. If $\epsilon_{\text{ff,meas}}$ is, for instance, high, one cannot say whether this stems from a high $\epsilon_{\text{ff,int}}$ or from an initially steep profile (see Equation 2). In addition, the initial gas density profile has been modified, especially in the clump inner regions, precisely the regions boosting early star

formation. Therefore, the current gas density profile of a star-forming clump cannot fully shed light on its past star formation history.

To make progress, we will introduce in Section 4 a method to estimate the intrinsic star formation efficiency per free-fall time of a star-forming clump, which does not require knowledge of its initial gas density profile. We will apply it to the model clumps calculated in Paper I, and we will show that it yields estimates of $\epsilon_{\text{ff,int}}$ which are in good agreement with the value actually used in the simulations (i.e. $\epsilon_{\text{ff,int}} = 0.01$). Once $\epsilon_{\text{ff,int}}$ has been estimated, the impact of the initial gas density profile can be recovered as the ratio $\zeta = \epsilon_{\text{ff,meas}}/\epsilon_{\text{ff,int}}$ (Equation 2). We now describe how we obtain the measured (global) star formation efficiency per freefall time of our model clumps.

3. TIME-AVERAGED MEASURED STAR FORMATION EFFICIENCY PER FREEFALL TIME

The measured star formation efficiency per freefall time depends on the clump gas mass m_{gas} and radius r_{clump} (whose combination yields the gas mean density $\langle \rho_{\text{gas}} \rangle$ and freefall time $\langle \tau_{\text{ff}} \rangle$), and on the clump star formation rate SFR_{clump} (Equation 1). In Paper I, SFR_{clump} refers to the instantaneous star formation rate, that is, the star formation rate at a given time t . However, for star-forming regions whose young stellar objects (YSO) can be counted, observers often obtain time-averaged star formation rates by combining the total mass in YSOs, m_{YSO} , with an assumed duration of the star formation episode t , i.e. $\langle SFR_{\text{clump}} \rangle = m_{\text{YSO}}/t$. We therefore introduce a more practical definition of the measured star formation efficiency per freefall time

$$\epsilon_{\text{ff,meas},\Delta t} = \frac{m_{\text{stars}}}{t} \times \frac{\langle \tau_{\text{ff}} \rangle}{m_{\text{gas}}}. \quad (5)$$

In the right-hand-side, m_{stars} is the stellar mass built by the model clump within the time-span t . The subscript Δt in the left-hand-side indicates that the measured star formation efficiency per freefall time now builds on a time-averaged star formation rate. Given that the instantaneous star formation rate of the model clumps decreases with time (see Figure 4 in Paper I), the advantage of using a time-averaged star formation rate is that it keeps track of the more vigorous star formation activity experienced at earlier times, thereby better preserving the impact of the initial gas density profile. This is $\epsilon_{\text{ff,meas},\Delta t}$ that we will compare to our estimates of the intrinsic star formation efficiency per freefall time (in Section 5). We now move into how to reveal the latter.

4. SPATIALLY-RESOLVED OBSERVATIONS TO THE RESCUE

4.1. Core of the method

Global observations of a clump with a gas density gradient can only yield its *measured* star formation efficiency per free-fall time (see Equation 1). To estimate its intrinsic star formation efficiency per free-fall time, one would ideally have at one's disposal a second clump containing the same gas mass distributed within the same radius, but according to a top-hat profile. Its star formation

rate SFR_{TH} would be measured and its star formation efficiency per freefall time would be inferred as:

$$\epsilon_{\text{ff,int}} = \frac{SFR_{\text{TH}} \langle \tau_{\text{ff}} \rangle}{m_{\text{gas}}}. \quad (6)$$

However, Nature does not offer us the top-hat equivalent of any star-forming clump we observe, and a method different from that building on Equation 1 needs to be elaborated.

While the measured star formation efficiency per freefall time characterizes the star formation activity of the clump globally, the intrinsic star formation efficiency per freefall time that we seek to estimate characterizes the star formation activity of the clump shells, from its edge to its center (see Equation 4 in Paper I). A seemingly naive approach is thus to focus on one of these shells. We will do just that. Specifically, we target the shell whose initial gas density is the clump mean density. We refer to this shell as the "mean shell". Its density is also the density ρ_{TH} of a top-hat model with identical clump mass m_{clump} and radius r_{clump} . We can write, with r_m the mean shell radius, $\rho_{\text{clump}}(r_m)$ the initial gas density of the mean shell, and ρ_{TH} the density of the top-hat model:

$$\rho_{\text{TH}} = \frac{m_{\text{clump}}}{\frac{4\pi}{3} r_{\text{clump}}^3} = \rho_{\text{clump}}(r_m). \quad (7)$$

In the model of Parmentier & Pflanzner (2013), the volume density in stars depends on the initial gas density, on the intrinsic star formation efficiency per freefall time $\epsilon_{\text{ff,int}}$ and on the star formation time-span t (see their Equations 19 and 20). That is, the longer the star formation duration t , the higher the intrinsic star formation efficiency per freefall time $\epsilon_{\text{ff,int}}$ and/or the higher the initial gas density (hence the shorter the gas initial freefall time), the faster the gas gets converted into stars and the lower/higher the gas/star density at time t . Given that the mean shell and the top-hat model have the same initial gas density, they evolve at the same pace *provided their intrinsic star formation efficiency per free-fall time $\epsilon_{\text{ff,int}}$ is the same*.

This is illustrated in the top panel of Figure 1, which shows the evolution of a gas density profile with $p_0 = 3$ (i.e. an initially steep density gradient) and of a top-hat model with the same clump mass, radius and intrinsic star formation efficiency per freefall time. Model parameters are $m_{\text{clump}} = 3.2 \cdot 10^4 M_{\odot}$, $r_{\text{clump}} = 1 \text{ pc}$, and $\epsilon_{\text{ff,int}} = 0.01$, combined to a gas initial density profile of steepness $p_0 = 3$ and central density $\rho_c = 7 \cdot 10^6 M_{\odot} \cdot \text{pc}^{-3}$. The clump mean volume density ($\simeq 8000 M_{\odot} \cdot \text{pc}^{-3}$) therefore falls in the density regime for which steep radial density profiles have been observed in molecular clouds of the Galactic disk (i.e. $10^4 \text{ cm}^{-3} < n_{\text{H}_2} < 3 \cdot 10^5 \text{ cm}^{-3} \equiv 700 M_{\odot} \cdot \text{pc}^{-3} < \langle \rho_{\text{clump}} \rangle < 2.1 \cdot 10^4 M_{\odot} \cdot \text{pc}^{-3}$; Schneider et al. 2015). The darkest line with open circles depicts the initial gas density profile $\rho_{\text{clump}}(r) = \rho_{\text{gas}}(r, t = 0)$ and the horizontal darkest line (best visible in the zoom-in region) is the top-hat model. The vertical dashed line marks the radius r_m of the mean shell, that is, the radius at which the clump density profile equates the top-hat density (as indicated by the downward green arrows). At any given time t of their evolution, the mean shell

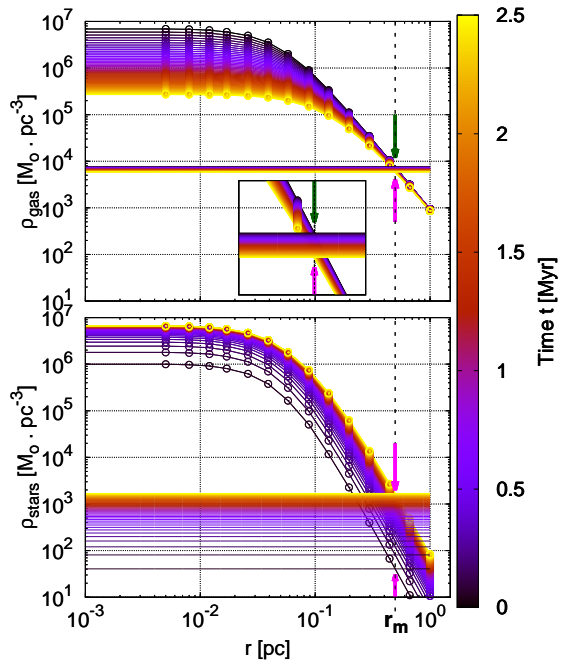


FIG. 1.— Top panel: Evolution with time of the gas density profile of two model clumps, one with a top-hat density profile (symbol-free lines), the other with an initial steepness $p_0 = 3$ (lines with open circles). The time t since star formation onset is color-coded by the right-hand-side palette. Model parameters are: $m_{clump} = 3.2 \cdot 10^4 M_\odot$, $r_{clump} = 1$ pc, $\epsilon_{ff,int} = 0.01$, and $\rho_c = 7 \cdot 10^6 M_\odot \cdot pc^{-3}$. The region where the local gas densities of both models are initially equal (i.e. the mean shell; green arrows) is zoomed-in. The vertical dashed line indicates the radial position of the mean shell (radius r_m). The magenta arrow indicates that both densities have remained equal to each other by $t = 2.5$ Myr. Bottom panel: same for the evolution of the stellar density profiles. The magenta arrows indicate that the stellar density of the top-hat model and the stellar density of the mean shell of the $p_0 = 3$ model are equal all through the simulations, from $t = 0.05$ Myr to $t = 2.50$ Myr.

and the top-hat profile keep presenting the same gas volume density because of their common intrinsic star formation efficiency per freefall time and common initial gas density. The upward magenta arrows highlight the equality at $t = 2.5$ Myr (best visible in the zoom-in region). Similarly, the mean shell and the top-hat profile present the same stellar density at any time t (see bottom panel of Figure 1 which shows the rise with time of the stellar density profiles of both models).

Knowledge of the radial position r_m of the mean shell is not needed, however. Only its gas- and star-volume densities are. In the next section, we therefore move to the $(\rho_{gas}, \rho_{stars})$ space.

4.2. From radial density profiles to star formation relations

The top panel of Figure 2 shows the volume-density-based star formation relation for several model clumps, which is the stellar density ρ_{stars} in dependence of the gas density ρ_{gas} . We refer to this relation as a *local* star formation relation, since the gas and star densities are those at given distances of the clump center (i.e. $(\rho_{gas}(r), \rho_{stars}(r))$), rather than densities averaged over the whole clump. The top-right end of a

relation corresponds to the clump central regions, while the lower-left end depicts the clump outskirts. All four clumps have the same mass ($m_{clump} = 3.2 \cdot 10^4 M_\odot$), radius ($r_{clump} = 1$ pc), star formation time-span ($t = 0.5$ Myr), intrinsic star formation efficiency per freefall time ($\epsilon_{ff,int} = 0.01$), but four distinct density profiles initially, namely $p_0 = 0, 2, 3$ and 4 . At the clump center, a core radius of $r_c = 0.02$ pc is initially imposed and the gas initial central density ρ_c is adjusted such that the radius r_{clump} contains the mass m_{clump} . As the density gradient steepens, the densities in the clump inner regions increase, while those in the clump outskirts decrease. This results in stretching out the relation as p_0 increases. Each density profile has a mean shell, and all three mean shells have the same initial gas density, which is that of the top-hat model ($p_0 = 0$). The top-hat model (orange plain diamond) therefore identifies the location of the mean shell of each centrally-concentrated clump in the $(\rho_{gas}, \rho_{stars})$ space. That is, it marks the location of a clump region which evolves at the same pace as the top-hat model. Their evolution is dictated by the *intrinsic* star formation efficiency per freefall time, not by the *global/measured* one.

If one runs another top-hat model with the same star formation time-span t but too high (too low) an intrinsic star formation efficiency per free-fall time, then that top-hat model finds itself above (below) the clump local star formation relations. This is illustrated by the open diamonds for which the intrinsic efficiency is 5 times higher (lower) than used for the $p_0 = (2, 3, 4)$ models. Therefore, the top panel of Figure 2 illustrates that if the initial mean density of a clump and the time elapsed since star formation onset are known, its intrinsic star formation efficiency per freefall time can be recovered by comparing its local star formation relation to the predictions made for top-hat models of various intrinsic efficiencies $\epsilon_{ff,int}^{TH}$. Knowledge of the initial gas density profile is not required. A limitation of the method as it is now, however, is that it builds on volume densities, while the densities directly measured by observers are surface densities. Therefore, we now move to the space of projected star and gas local densities $(\Sigma_{gas}, \Sigma_{stars})$.

4.3. From volume densities to surface densities

Spatially-resolved observations of molecular clouds have revealed their local star formation relation, namely, the relation between the local surface density in young stars and the local surface density of the gas. As for the model volume densities above, we coin those surface densities "local" because they are measured at the location of individual proto- or pre-main-sequence stars (e.g. Gutermuth et al. 2011), or measured within given gas-surface-density contours (e.g. Heiderman et al. 2010). They are not averaged over an entire cloud or clump. With the advent of the Atacama Large Millimeter Array, such diagnostic plots are now also collected for molecular clouds of the Central Molecular Zone (e.g. Ginsburg et al. 2018).

The bottom panel of Figure 2 presents the projected local star formation relations $(\Sigma_{gas}, \Sigma_{stars})$ of the models shown in the top panel. The orange rectangle depicts the top-hat model which, as in the top panel, overlaps with the $p_0 \neq 0$ models as a result of their common star for-

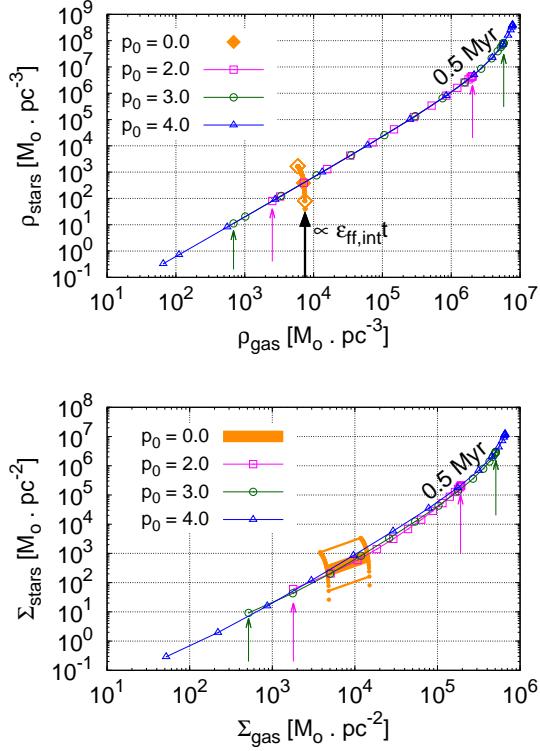


FIG. 2.— Top panel: Star formation relations of model clumps based on their local volume densities in stars and gas. Model parameters are $m_{clump} = 3.2 \cdot 10^4 M_{\odot}$, $r_{clump} = 1 \text{ pc}$, $r_c = 0.02 \text{ pc}$, $\epsilon_{\text{ff,int}} = 0.01$, and $t = 0.5 \text{ Myr}$, and p_0 varying from 0 (top-hat profile) to $p_0 = 4$ (very steep profile; see the key). The extent of the $p_0 = (2, 3)$ models is shown by the thin vertical arrows, color-coded accordingly. The orange open diamonds indicate the locus of the top-hat model when $\epsilon_{\text{ff,int}}^{TH} = 5\epsilon_{\text{ff,int}} = 0.05$ and $\epsilon_{\text{ff,int}}^{TH} = \epsilon_{\text{ff,int}}/5 = 0.002$. The track of orange plain circles indicate the time-evolution of the model with $\epsilon_{\text{ff,int}}^{TH} = 0.01$ from $t = 0.05 \text{ Myr}$ up to $t = 2.5 \text{ Myr}$. Bottom panel: Same as top panel, but based on the local surface densities in stars and gas. The orange plain rectangle, the upper and lower orange thick lines indicate, respectively, the locations of the top-hat model at $t = 0.5 \text{ Myr}$ when $\epsilon_{\text{ff,int}}^{TH} = 0.01, 0.05$ and 0.002 .

mation time-span, common gas initial mean density, and common intrinsic star formation efficiency per free-fall time. The thick orange lines above and beneath it depict the models with $\epsilon_{\text{ff,int}}^{TH} = 5\epsilon_{\text{ff,int}}$ and $\epsilon_{\text{ff,int}}^{TH} = \epsilon_{\text{ff,int}}/5$.

The concept is further illustrated in Figure 3. Each of its four panels compares (i) the local star formation relation of a clump with a steep density gradient (either $p_0 = 3$ or $p_0 = 4$) and an intrinsic star formation efficiency per freefall time $\epsilon_{\text{ff,int}} = 0.01$ to (ii) a grid of relations obtained for a uniform-density clump ($p_0 = 0$) with identical initial gas mass, radius, star formation time-span, but different intrinsic star formation efficiencies per free-fall time. The clump mass and radius, the time-span since star formation onset, and the density gradient of the centrally-concentrated clump are quoted in each panel. Both types of models ($p_0 = 0$ and $p_0 = (3, 4)$) are easily distinguishable based on their distinct extent in the $(\Sigma_{\text{gas}}, \Sigma_{\text{stars}})$ space. All relations are color-coded as a function of the distance r from the clump center. In that respect note that each color palette

has its own upper limit, to reflect the size of each model clump. The intrinsic star formation efficiency per freefall time of the top-hat models ranges from $\epsilon_{\text{ff,int}}^{TH} = 10^{-4}$ to 10 in logarithmic steps of 0.5 (value quoted to the right of every two relations). As $\epsilon_{\text{ff,int}}^{TH}$ increases (while retaining the same star formation time-span t), the corresponding star formation relation moves to higher star- and lower gas-surface densities, highlighting thereby a faster pace of star formation for higher star formation efficiencies per free-fall time. Also quoted in each panel is the measured star formation efficiency per free-fall time of the centrally-concentrated clump $\epsilon_{\text{ff,meas},\Delta t}$ (see Section 3). It sometimes differs from its intrinsic counterpart $\epsilon_{\text{ff,int}} = 0.01$ by more than an order of magnitude. Nevertheless, a mere visual inspection of the diagrams yields an estimate of the intrinsic star formation efficiency per free-fall time for the $p_0 = (3, 4)$ models. This one is revealed by the top-hat model whose local star formation relation best overlaps the clump model with a steep, but unknown, initial density gradient. We refer to the $\epsilon_{\text{ff,int}}$ estimate as the corrected star formation efficiency per free-fall time, $\epsilon_{\text{ff,cor}}$. The method yields $\epsilon_{\text{ff,cor}} \simeq 0.01$ for each of the four cases, in agreement with the intrinsic efficiency actually used in the simulations, i.e. $\epsilon_{\text{ff,int}} = 0.01$. Resolved observations hold therefore the potential to deliver the right order-of-magnitude for $\epsilon_{\text{ff,int}}$, while the measured efficiency provided by global observations can be off by an order-of-magnitude, or more.

5. APPLICATION OF THE METHOD

We have applied the method devised in Section 4.3 to all the model clumps with $p_0 = 3$ and $p_0 = 4$ computed in Paper I. When $p_0 \geq 3$, the ratio between the (instantaneous) measured star formation efficiency per freefall time and its intrinsic counterpart can reach 3 orders of magnitude (equivalently the magnification factor can reach $\zeta(t) \gtrsim 10^3$; see e.g. bottom-right panel of Figure 5 in Paper I). This is therefore the regime where an estimate of $\epsilon_{\text{ff,int}}$ is the most needed. Models with $p_0 \geq 3$ are of two types (Sections 5.1 and 5.2 of Paper I, respectively). In a first category, the central core radius r_c of the gas initial density profile is imposed ($r_c = 0.02 \text{ pc}$) and the clump central density ρ_c is calculated such that the clump radius r_{clump} contains the assigned clump mass m_{clump} . In a second category, this is the central density ρ_c of the initial gas density profile which is imposed ($\rho_c = 7 \cdot 10^6 M_{\odot} \cdot \text{pc}^{-3}$) and the corresponding core radius r_c is inferred such that the clump radius r_{clump} contains the clump mass m_{clump} . In most cases, the first category yields higher magnification factors because the absence of constraint on the central density leads to greater density contrasts between the clump center and the clump edge. Magnification factors predicted for clumps whose initial gas central density is imposed are in contrast smaller, especially for massive clumps (compare e.g. the bottom-right panel of Figure 5 with the top-right panel of Figure 7 in Paper I). This is because a compact massive clump with a limited central density necessarily presents a wide central core to accommodate its large mass m_{clump} inside its given radius r_{clump} . As a result, the impact of the steep density profile in the outer regions is counteracted by the significant flat density profile in the inner regions.

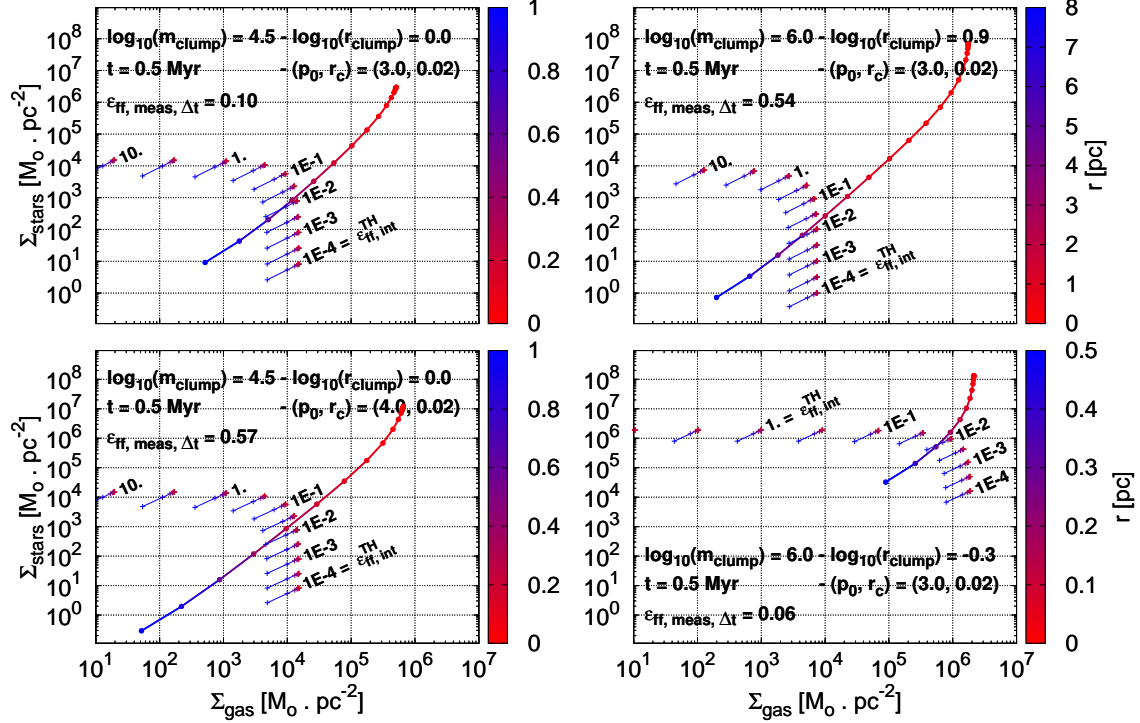


FIG. 3.— For each panel, comparison between the star formation relation of a centrally-concentrated clump and a grid of star formation relations for top-hat models. Common model parameters are the radius r_{clump} , enclosed mass m_{clump} and star formation time-span t . They are quoted in each panel, along with the parameters (p, r_c) of the gas initial density profile of the centrally-concentrated clump. Also given is its measured star formation efficiency per freefall time $\epsilon_{\text{ff, meas}, \Delta t}$ as defined by Equation 5 (i.e. based on a time-averaged star formation rate). The star formation relations of the top-hat models have been calculated for intrinsic star formation efficiencies per free-fall time $\epsilon_{\text{ff, int}}^{TH}$ ranging from 10^{-4} to 10, in logarithmic steps of 0.5 as quoted next to every two relations. The comparison of both types of star formation relation yields an estimate of the intrinsic star formation efficiency per freefall time of the centrally-concentrated clump ($\epsilon_{\text{ff, int}} = 0.01$ in all simulations). All relations are color-coded as a function of the distance r to the clump center, each color palette having its own extent as given by the corresponding clump radius.

The model clumps that we consider therefore present a wide range of gas initial density profiles (hence of values of the initial magnification factor ζ), in addition to large ranges of clump radii (from 0.5 to 8 pc), initial gas masses (from 300 to $10^6 M_{\odot}$), and star formation time-spans (up to 2.5 Myr after star formation onset).

The left panels of Figure 4 present the measured star formation efficiency per freefall time $\epsilon_{\text{ff, meas}, \Delta t}$ (Equation 5) for model clumps with the initial core radius r_c imposed. The initial steepness of the gas density profile is either $p_0 = 3$ (top panel) or $p_0 = 4$ (bottom panel). The star formation time-span, the initial core radius and the intrinsic star formation efficiency per freefall time are: $t = 0.5$ Myr, $r_c = 0.02$ pc and $\epsilon_{\text{ff, int}} = 0.01$. The measured star formation efficiency per freefall time is given by the symbol color coding (see right-hand-side palette). Note that this one is logarithmic and covers three orders of magnitude, from $\epsilon_{\text{ff, meas}, \Delta t} = 0.01$ up to $\epsilon_{\text{ff, meas}, \Delta t} = 10$. The lower limit thus corresponds to the intrinsic star formation efficiency per free-fall time actually used in the simulations. As discussed in Paper I, the measured star formation efficiency per freefall time gets higher if, all other parameters being kept the same, the initial density profile gets steeper (higher p_0), or if the r_c/r_{clump} ratio gets smaller, or if the clump mass gets lower (hence a lower volume density and a slower

decrease with time of the magnification factor). Plain circles (triangles) depict models which have converted less (more) than half of their initial gas mass into stars by the elapsed time-span $t = 0.5$ Myr.

The right panels present, for the same parameter space, the corrected star formation efficiency per free-fall time $\epsilon_{\text{ff, cor}}$, that is, the estimate of the intrinsic star formation efficiency per freefall time recovered through the method illustrated in Figure 3. Given a sequence of intrinsic efficiencies ($\epsilon_{\text{ff, int}}^{TH} = 0.005$ to 0.10 in steps of 0.005), the corresponding grid of top-hat models is built and the one model minimizing the vertical distance between its star formation relation and that of the centrally-concentrated clump yields the best estimate $\epsilon_{\text{ff, cor}}$. The vertical distance is measured at the mean gas surface density of the top-hat model. For the sake of comparison, the same color coding is used in the left and right panels. In contrast to the left panels, the color of the symbols in the right panels is almost uniformly deep-blue or purple, indicating that the method has successfully recovered the intrinsic star formation efficiency per free-fall time, that is, $\epsilon_{\text{ff, cor}} \simeq \epsilon_{\text{ff, int}} = 0.01$. This holds regardless of the initial steepness of the density profile, of the clump mass, or of the clump radius. This also holds independently of how advanced the star formation process is since the right panels show $\epsilon_{\text{ff, cor}} \simeq \epsilon_{\text{ff, int}}$ for both the triangles

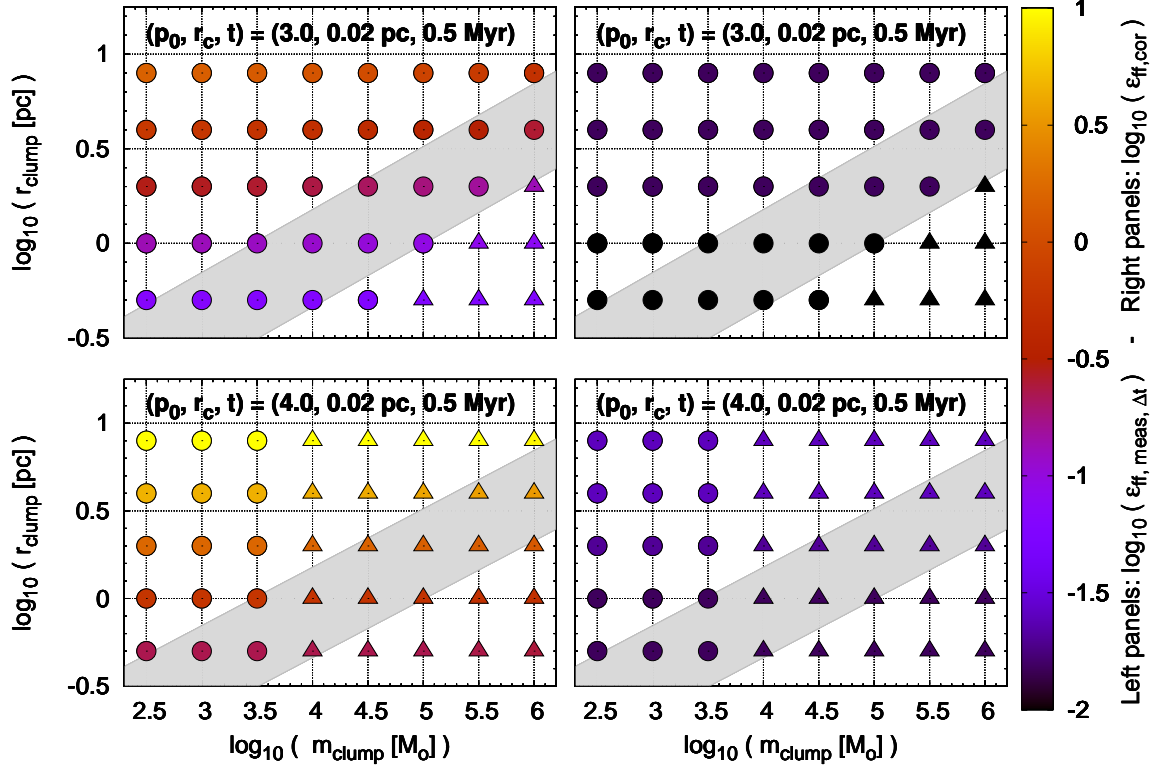


FIG. 4.— Comparison between the measured star formation efficiency per free-fall time of our model clumps ($\epsilon_{\text{ff,meas},\Delta t}$, left panels) and our estimates of their intrinsic efficiency ($\epsilon_{\text{ff,cor}}$, right panels) with the initial core radius imposed. Parameters are the radius and initial gas mass of clumps, r_{clump} and m_{clump} , and the initial steepness p_0 of their density profile (top panels: $p_0 = 3$; bottom panels: $p_0 = 4$). The initial core radius and the intrinsic star formation efficiency per freefall time are set to $r_c = 0.02$ pc and $\epsilon_{\text{ff,int}} = 0.01$. Each model is represented by a plain symbol, the color of which depicts the value of the corresponding efficiency (see palette for color-coding, with a logarithmic scale). The grey stripe highlights the density regime $10^4 \text{ cm}^{-3} < n_{\text{H}2} < 3 \cdot 10^5 \text{ cm}^{-3} \equiv 700 M_{\odot} \cdot \text{pc}^{-3} < \langle \rho_{\text{clump}} \rangle < 2.1 \cdot 10^4 M_{\odot} \cdot \text{pc}^{-3}$ for which steep density profiles have been detected in Galactic clouds (Schneider et al. 2015). Model clumps which by $t = 0.5$ Myr have achieved $SFE_{\text{gl}} > 0.50$ are depicted by triangles.

($SFE_{\text{gl}} > 0.50$) and the circles ($SFE_{\text{gl}} < 0.50$).

Figure 5 presents the equally-good results for clumps with the initial gas central density imposed. As reminded earlier in this section, such clumps often present less extreme magnification factors and convert therefore over the same time-span t a smaller fraction of their gas mass into stars (that is, triangles are less numerous in Figure 5 than in Figure 4).

The total number of tested models amounts to 8000, corresponding to 8 clump masses, 5 radii, 50 star formation time-spans, 2 initial steepnesses p_0 of the density profile, and 2 different constraints for the initial gas density profile (either imposed central core radius, or imposed central density). The corrected efficiency differs from the intrinsic efficiency actually used in the simulations by at most a factor of three (i.e. $\epsilon_{\text{ff,int}} = 0.01 \leq \epsilon_{\text{ff,cor}} \leq 0.03$: see Figure 6). This constitutes a great improvement over the globally-measured star formation efficiency per freefall time shown in the left panels of Figures 4 and 5, where some of these are higher than unity.

With an estimate of $\epsilon_{\text{ff,int}}$ secured, the impact of the initial gas density profile on the clump star formation

history can be recovered as the ratio

$$\zeta_{\text{estimate}} = \frac{\epsilon_{\text{ff,meas},\Delta t}}{\epsilon_{\text{ff,cor}}}, \quad (8)$$

with $\epsilon_{\text{ff,meas},\Delta t}$ the "traditional" estimate of the star formation efficiency per free-fall time.

6. HOW TO IMPLEMENT THE METHOD

In this section, we provide the equations needed to build the "ladder" of star formation relations for top-hat profiles, such as those shown in Figure 3. We then detail how to implement the method in a step-by-step way.

6.1. Local star-formation relations of top-hat profiles

For homogeneous models, star formation proceeds at the same pace everywhere (i.e. $\tau_{\text{ff}}(r)$ is independent of the distance r from the clump center). Therefore, the gas retains a top-hat volume density profile (Figure 1), and the forming star cluster has a top-hat volume density profile too. To build the projected local star formation relation, we need the gas and star surface density profiles. When both $\rho_{\text{gas}}(r)$ and $\rho_{\text{stars}}(r)$ are independent of r ,

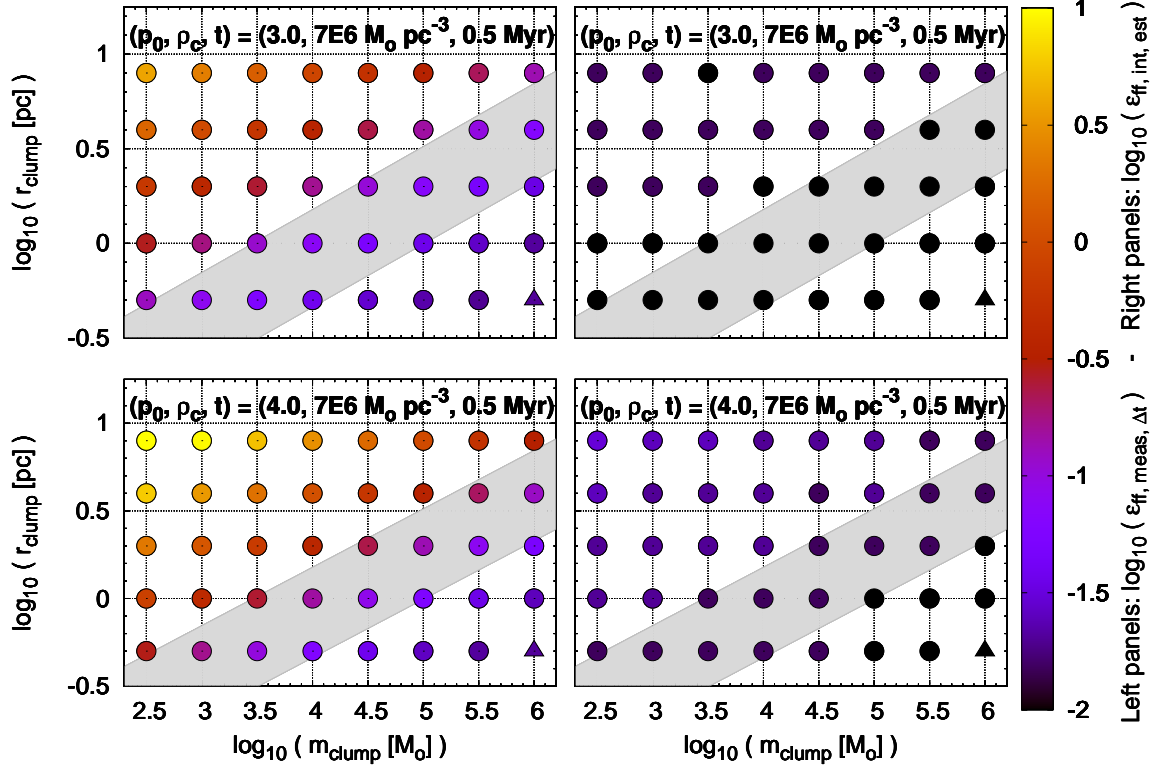


FIG. 5.— Same as Figure 4, but with the initial central density of the clump gas imposed: $\rho_c = 7 \cdot 10^6 M_\odot \cdot \text{pc}^{-3}$

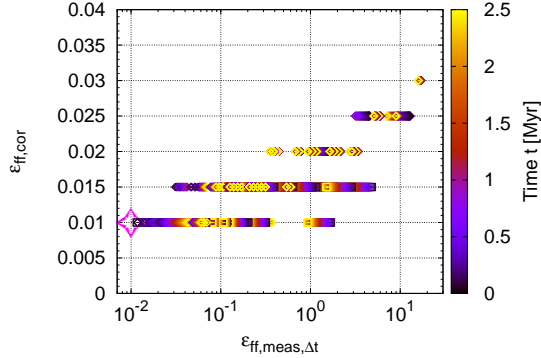


FIG. 6.— Comparison between the measured star formation efficiency per freefall time $\epsilon_{\text{ff,meas},\Delta t}$ and our estimate $\epsilon_{\text{ff,cor}}$ of its intrinsic counterpart for all tested models. The time t of the model is color-coded by the right-hand-side palette. Note the logarithmic scale of the x -axis and the linear scale of the y -axis. The magenta four-branch star indicates the intrinsic efficiency actually used in the simulations, $\epsilon_{\text{ff,int}} = 0.01$

the surface density profiles are given by

$$\Sigma_{\text{gas}}(r, dr) = \frac{[r_{\text{clump}}^2 - (r - dr)^2]^{3/2} - [r_{\text{clump}}^2 - r^2]^{3/2}}{r_{\text{clump}} \cdot dr \cdot (2r - dr)} \frac{m_{\text{gas}}^{\text{TH}}}{\pi r_{\text{clump}}^2}, \quad (9)$$

and

$$\Sigma_{\text{stars}}(r, dr) = \frac{[r_{\text{clump}}^2 - (r - dr)^2]^{3/2} - [r_{\text{clump}}^2 - r^2]^{3/2}}{r_{\text{clump}} \cdot dr \cdot (2r - dr)} \frac{m_{\text{stars}}^{\text{TH}}}{\pi r_{\text{clump}}^2}. \quad (10)$$

In these equations, Σ_{gas} and Σ_{stars} are the gas and star surface densities measured inside an annulus of inner and outer radii $r - dr$ and r . $m_{\text{gas}}^{\text{TH}}$ and $m_{\text{stars}}^{\text{TH}}$ are, respectively, the gas and stellar masses of the top-hat model. We recall that in the method illustrated in Figure 3, top-hat models and the centrally-concentrated clump for which an estimate of $\epsilon_{\text{ff,int}}$ is sought have the same (mean) volume density. We therefore assign them the same radius and total mass (i.e. $r_{\text{clump}} = r_{\text{clump}}^{\text{TH}}$ and $m_{\text{clump}} = m_{\text{clump}}^{\text{TH}}$), which implies that: $m_{\text{gas}}^{\text{TH}} + m_{\text{stars}}^{\text{TH}} = m_{\text{clump}}^{\text{TH}} = m_{\text{clump}} = m_{\text{gas}} + m_{\text{stars}}$.

Equations 9 and 10 show that three parameters are needed to build the local star formation relation: r_{clump} , $m_{\text{gas}}^{\text{TH}}$ and $m_{\text{stars}}^{\text{TH}}$. While observing the centrally-concentrated clump can provide estimates of r_{clump} and m_{clump} , the gas and stellar masses at time t of the top-hat model, $m_{\text{gas}}^{\text{TH}}$ and $m_{\text{stars}}^{\text{TH}}$, have to be predicted. That is, given a model clump of radius r_{clump} , initial gas mass m_{clump} and density profile steepness $p_0 = 0$, what are its stellar mass $m_{\text{stars}}^{\text{TH}}$ and gas mass $m_{\text{gas}}^{\text{TH}}$ at time t given an intrinsic star formation efficiency per freefall time $\epsilon_{\text{ff,int}}^{\text{TH}}$? Since the radius of the clump, thus its vol-

ume, is known, we simply need the gas and star volume densities. These are predicted by Equations 19 and 20 of Parmentier & Pflanzner (2013) which, for an initial uniform gas density ρ_{TH} , become

$$\begin{aligned} \rho_{gas}^{TH}(t) &= \left(\rho_{TH}^{-1/2} + \sqrt{\frac{8G}{3\pi}} \cdot \epsilon_{ff,int}^{TH} \cdot t \right)^{-2} \\ &= \rho_{TH} \left(1 + \frac{1}{2} \frac{\epsilon_{ff,int}^{TH} \cdot t}{\tau_{ff}(t=0)} \right)^{-2}, \end{aligned} \quad (11)$$

and

$$\rho_{stars}^{TH}(t) = \rho_{TH} - \rho_{gas}^{TH}(t). \quad (12)$$

The initial gas density ρ_{TH} is known since it equates the mean density of the centrally-concentrated clump (ρ_{clump}):

$$\rho_{TH} = \frac{m_{clump}}{\frac{4\pi}{3} r_{clump}^3} = \langle \rho_{clump} \rangle, \quad (13)$$

and $\tau_{ff}(t=0)$ is the free-fall time corresponding to ρ_{TH} .

The masses m_{gas}^{TH} and m_{stars}^{TH} then follow from Equations 11 and 12 as:

$$m_{gas}^{TH}(t) = \rho_{gas}^{TH}(t) \frac{4\pi}{3} r_{clump}^3, \quad (14)$$

and

$$m_{stars}^{TH}(t) = \rho_{stars}^{TH}(t) \frac{4\pi}{3} r_{clump}^3. \quad (15)$$

The gas and star projected density profiles of the top-hat model at time t can now be obtained following Equations 9 and 10, and the local star formation relation follows from plotting the star projected density as a function of its gas equivalent.

6.2. Step-by-step application of the method

The method to estimate the intrinsic star formation efficiency per freefall time of a centrally-concentrated clump unfolds as follow:

- Estimate the radius r_{clump} of the centrally-concentrated clump. Under the assumption that the clump is in dynamical equilibrium, this is also the clump initial radius;
- Estimate the total mass $m_{clump} = m_{gas} + m_{stars}$ enclosed within r_{clump} . Under the assumption that the clump is isolated, the total mass is also the initial gas mass;
- Estimate the time t elapsed since star formation onset in the centrally-concentrated clump;
- t , r_{clump} and m_{clump} are also the parameters adopted for the top-hat models whose local star formation relations now need to be built; each star formation relation corresponds to one tested value of the intrinsic star formation efficiency per freefall time $\epsilon_{ff,int}^{TH}$;
- For a given $\epsilon_{ff,int}^{TH}$, Equations 11 and 12 predict the corresponding gas and star volume densities of the top-hat model following a star formation time-span t (the initial gas volume density ρ_{TH} is known from Equation 13);
- The star and gas masses hosted by the top-hat model at time t are then given by Equations 14 and 15;
- The local star formation relation can now be built as

a parametric plot of Equations 9 and 10;

- The above is to be repeated for a sequence of intrinsic star formation efficiencies per freefall time $\epsilon_{ff,int}^{TH}$, which results in a grid of local star formation relations like those shown in Figure 3.

- Comparing the just obtained model grid with the local star formation relation of the observed centrally-concentrated clump yields an estimate of its intrinsic star formation efficiency per free-fall time.

7. DISCUSSION

7.1. t -Uncertainties propagate as $\epsilon_{ff,int}$ -uncertainties

Equations 19 and 20 in Parmentier & Pflanzner (2013) show that, for a given gas initial volume density, the evolutionary stage depends on the product of the star formation efficiency per freefall time and of time, $\epsilon_{ff,int}t$ (see also Figure 2). That is, moving a star formation episode "forward" can be done either by considering a longer star formation time-span, or by adopting a higher intrinsic star formation efficiency per free-fall time. Similarly, Equation 11 shows that the key parameter associated to each star formation relation of the top-hat grid is not $\epsilon_{ff,int}^{TH}$, but the product $\epsilon_{ff,int}^{TH} \cdot t$. In Figure 3, we have inferred that the best solution is always provided by the "rung" corresponding to $\epsilon_{ff,int}^{TH} = 0.01$, namely, the rung which is the closest to the star formation relation of the centrally-concentrated clump (see also bottom panel of Figure 2). However, this holds only if the star formation time-span t has been reliably estimated ($t = 0.5$ Myr in Figure 3). If it has been overestimated by, say, a factor of 4 (i.e. $t_{obs} = 2$ Myr, with t_{obs} the assumed star formation time-span), then the star formation efficiency per freefall time is underestimated by a factor of 4 and $\epsilon_{ff,cor} \simeq 0.0025$. Conversely, underestimating the star formation time-span by, say, a factor of 5 (i.e. $t_{obs} = 0.1$ Myr is assumed) results in overestimating the star formation efficiency per free-fall time, in this case by a factor of 5 and $\epsilon_{ff,cor} \simeq 0.05$. In fact, all top-hat models with $\epsilon_{ff,cor}t_{obs} = \epsilon_{ff,int}t = 0.01 \cdot 0.5 = 0.005$ Myr provide good matches of the local star formation relation of the centrally-condensed clump. Uncertainties in the assumed star formation duration are therefore directly reflected as uncertainties in the intrinsic star formation efficiency per freefall time.

7.2. Clouds vs. Clumps

At this stage, it is important to note that the method has been devised for *individual* molecular clumps, *not* for entire molecular clouds. Molecular clouds consist of diffuse gas in which several denser molecular clumps are embedded. The mean volume density may vary from clump to clump, implying that the clumps have different freefall times and evolutionary paces. They may also have started to form stars at different times. As a result, the local star formation relation of a molecular cloud is an assembly of local star formation relations corresponding to star-forming sites at different evolutionary stages, yielding thereby different vertical locations in the $(\Sigma_{gas}, \Sigma_{stars})$ parameter space. The local star formation relation of a cloud can thus be severely thickened and "blurred" (see e.g. Figure 6 in

Parmentier 2014), thereby preventing a proper comparison with a grid of top-hat models. This effect pops up nicely when comparing the observed local star formation relations of the Orion and Ophiuchus molecular clouds, as obtained by Gutermuth et al. (2011). While the stellar content of the Ophiuchus cloud is dominated by one embedded cluster (their Figure 6), the Orion cloud is a large collection of numerous individual star-forming regions (their Figure 4). The result for Ophiuchus is a fairly neatly defined local star formation relation, while the star formation relation of the Orion molecular cloud looks like a broad cloud of points, almost two orders of magnitude thick in stellar surface density (their Figure 9). It is therefore crucial that observers, when collecting local surface densities of gas and stars for molecular clouds, split their data into well-defined star-forming sites corresponding to the smaller-scale of denser molecular clumps. Only then can the method be meaningfully applied to observational data sets. Should the mass and size of these clumps be known, it then becomes possible to constrain their evolutionary stage (the $\epsilon_{\text{ff,int}} t$ parameter) by matching them to top-hat models such as those described in this paper.

8. CONCLUSIONS

Molecular clumps have a higher star formation rate when they present a volume density gradient than when they are uniform in density (Tan et al. 2006; Girichidis et al. 2011; Cho & Kim 2011; Elmegreen 2011; Parmentier 2014, 2019). This implies that the star formation efficiency per freefall time that is measured for such clumps (Equation 1) is also higher than what would be measured if their gas was of uniform density. This *measured* star formation efficiency per freefall time $\epsilon_{\text{ff,meas}}$ is a global quantity since it depends on the star formation rate of clumps, and on the mean density (hence freefall time) and mass of their gas. The efficiency of the clump top-hat equivalent is defined as the *intrinsic* star formation efficiency per freefall time $\epsilon_{\text{ff,int}}$. That is, this is the star formation efficiency per freefall time that would be measured if clumps had no gas density gradient. For a centrally-concentrated clump, the intrinsic efficiency $\epsilon_{\text{ff,int}}$ is also the efficiency characterizing the star formation activity of any clump region small enough to be considered of uniform density (i.e. a region that is small enough so that it does not "see" the clump density gradient). This is for instance the case of the individual spherically-symmetric shells of gas of which a clump is made (see Equation 4 in Parmentier 2019). The ratio between the measured (equivalently global) and intrinsic (equivalently local) star formation efficiencies per freefall time defines the so-called *magnification factor* ζ . Its name stems from ζ being also the ratio between the star formation rate of a centrally-concentrated clump and the star formation rate of its top-hat equivalent (see Equation 2 of this paper and Parmentier 2019). The implications are that, even for a fixed $\epsilon_{\text{ff,int}}$, its measured counterpart $\epsilon_{\text{ff,meas}}$ present wide variations, reflecting the diversity of clump inner structures rather than variations in the star formation process itself. Intrinsic and measured efficiencies are equal (similar) for top-hat (shallow) gas density profiles only.

That the degree of central concentration of a molec-

ular clump contributes to its measured star formation efficiency per free-fall time $\epsilon_{\text{ff,meas}}$, thereby masking the intrinsic efficiency $\epsilon_{\text{ff,int}}$ at work inside its constituent shells, leaves us with an annoying degeneracy. For instance, when the measured star formation efficiency per freefall time of a clump is high, one cannot *a priori* disentangle whether this results from a high intrinsic star formation efficiency per freefall time or from a clump steep density gradient. In the first case, the gas is highly efficient at forming stars, and would remain so even if the clump gas were of uniform density. In the second case, this is the clump gas central concentration, embodied by the magnification factor ζ , which drives the high measured star formation efficiency per freefall time of the clump.

In this paper, we have presented a method allowing one to lift this degeneracy. It builds on the local star formation relation, which relates the densities in gas and stars at a given radial location inside the star-forming clump (hence the term 'local'). The method requires therefore spatially-resolved observations of molecular clumps. Global (i.e. clump-averaged) data are not enough. The key idea on which the method hinges is that steepening the volume density profile of a clump, starting from a top-hat model, stretches out its local star formation relation while retaining the vertical normalization of the top-hat model (see top panel of Figure 2). This suggests that to estimate the intrinsic star formation efficiency per freefall time $\epsilon_{\text{ff,int}}$ of a centrally-concentrated clump, one can compare its local star formation relation with a grid of top-hat models of identical mass, radius, star formation time-span, but with their own star formation efficiencies per freefall time $\epsilon_{\text{ff,int}}^{TH}$. $\epsilon_{\text{ff,int}}$ follows from selecting the top-hat model which minimizes the vertical offset between its star formation relation and that of the centrally-concentrated clump. This property is also valid in the parameter space of gas- and star-surface densities (see bottom panel of Figure 2), making the method applicable to observational data sets. Knowledge of the clump gas initial density profile is not required. Only its total mass, radius and star formation time-span are. With these data, one can build the corresponding sequence of star formation relations for top-hat profiles (see the "ladders" made of star-formation relations in Figure 3).

We have systematically applied our method to the model clumps with an initially steep density profile calculated in Parmentier (2019). By "steep", we mean power-law density profiles with a logarithmic slope of -3 or steeper initially. Assuming that the star formation time-span is known, we recover, to better than a factor of 3, the intrinsic star formation efficiency per freefall time $\epsilon_{\text{ff,int}}$ actually used in the simulations. For comparison, it should be noted that $\epsilon_{\text{ff,meas}}$ differs from $\epsilon_{\text{ff,int}}$ by up to three orders-of-magnitude in the most centrally-concentrated models (see Figure 6). We have provided a step-by-step description of the method, and the equations that its implementation requires (Section 6). Uncertainties in the star formation time-span t are reflected as $\epsilon_{\text{ff,int}}$ -uncertainties since the clump evolutionary stage depends on their product (see Equation 19 in Parmentier & Pfalzner 2013). We stress that the method must be applied to individual molecular clumps, rather than to their host molecular clouds, given that clouds

consist of several clumps, each with its own star formation time-span and initial gas density. A collection of clumps therefore leads to "piling-up" several star formation relations (Section 7).

Once an estimate of the intrinsic star formation efficiency per freefall time $\epsilon_{\text{ff,int}}$ has been secured, it can be combined to the "traditional"/globally-measured star formation efficiency per freefall time $\epsilon_{\text{ff,meas}}$ to assess the impact that the gas density gradient of a clump has had on its star-formation history (Equation 8). Combining the method presented in this contribution with the spatial resolution of the Atacama Large Millimetre Array

will allow us to investigate whether the intrinsic star formation efficiency per freefall time of Galactic molecular clumps varies as a function of environment.

G.P. is grateful to Anna Pasquali and Douglas Heggie for stimulating discussions while working on this manuscript. G.P. acknowledges funding by the Deutsche Forschungsgemeinschaft (DFG, German Research Foundation – project-id 138713538 – SFB 881 ("The Milky Way System", subproject B05).

REFERENCES

- Cho, W., & Kim, J. 2011, *MNRAS*, 410, L8
 Elmegreen, B.G. 2011, *ApJ*, 731, 61
 Evans, J.E. II, Dunham, M.M., Jorgensen, J.K., Enoch, M.L., Merin, B. 2009, *ApJS*, 181, 321
 Ginsburg, A.; Bally, J.; Barnes, A.; Bastian, N.; Battersby, C. 2018, *ApJ*, 853, 171
 Girichidis, P., Federrath, C., Banerjee, R., Klessen, R.S. 2011, *MNRAS*, 413, pp2741-2759
 Gutermuth, R.A., Pipher, J.L., Megeath, S.T., et al. 2011, *ApJ*, 739, 84
 Heiderman, A.; Evans, N.J., II; Allen, L.E.; Huard, T.; Heyer, M. 2010, *ApJ* 723, 1019
 Krumholz, M.R., Tan, J.C. 2007, *ApJ*, 654, 304
 Krumholz, M.R., Dekel, A. & McKee, C.F. 2012, *ApJ*, 745, 69
 Lada, C.J., Lombardi, M., Alves, J.F. 2010, *ApJ*, 724, 687
 Motte, F., André, P., & Neri, R. 1998, *A&A*, 336, 150
 Motte, F., Bontemps, S., & Louvet, F. 2018, *ARA&A*, 56, 41
 Müller, K.E., Shirley, Y.L., Evans, N.J. II & Jacobson, H.R. 2002, *ApJS*, 143, 469
 Murray, N. 2011, *ApJ*, 729, 133
 Ochsendorf, B. B., Meixner, M., Roman-Duval, J., Rahman, M. & Evans, II, N.J. 2017, *ApJ*, 841, 109
 Parmentier, G., Pfalzner, S. 2013, *A&A*, 549, 132
 Parmentier, G. 2014, *Astronomische Nachrichten*, 335, 543
 Parmentier, G. 2019, *ApJ*, 887, 179
 Schneider, N., Bontemps, S., Girichidis, P., Rayner, T., Motte, F., et al 2015, *MNRAS*453, L41-L45
 Tan, J.C., Krumholz, M.R. & McKee, C.F. 2006, *ApJ*, 641, L121
 Vutisalchavakul, N.; Evans, N.J., II & Heyer, M. 2016, *ApJ*, 831, 73